

## Insulator Materials for Interface Passivation of Cu(In,Ga)Se-2 Thin Films

Peer-reviewed author version

Cunha, J. M. V.; Fernandes, P. A.; Hultqvist, A.; Teixeira, J. P.; Bose, S.;  
VERMANG, Bart; Garud, S.; BULDU KOHL, Dilara; Gaspar, J.; Edoff, M.; Leitao, J.  
P. & Salome, P. M. P. (2018) Insulator Materials for Interface Passivation of  
Cu(In,Ga)Se-2 Thin Films. In: IEEE JOURNAL OF PHOTOVOLTAICS, 8(5), p. 1313-1319.

DOI: 10.1109/JPHOTOV.2018.2846674

Handle: <http://hdl.handle.net/1942/28468>

# Insulator materials for interface passivation of Cu(In,Ga)Se<sub>2</sub> thin films

J. M. V. Cunha, P. A. Fernandes, A. Hultqvist, J. P. Teixeira, S. Bose, B. Vermang, S. Garud, D. Buldu, J. Gaspar, M. Edoff, J. P. Leitão and P. M. P. Salomé

**Abstract**— In this work, Metal-Insulator-Semiconductor (MIS) structures were fabricated in order to study different types of insulators, namely, aluminum oxide (Al<sub>2</sub>O<sub>3</sub>), silicon nitride (Si<sub>3</sub>N<sub>x</sub>) and silicon oxide (SiO<sub>x</sub>) to be used as passivation layers in Cu(In,Ga)Se<sub>2</sub> (CIGS) thin film solar cells. The investigated stacks consisted of SLG/Mo/CIGS/insulator/Al. Raman scattering and Photoluminescence measurements were done to verify the insulator deposition influence on the CIGS surface. In order to study the electrical properties of the CIGS-insulator interface, capacitance vs. conductance and voltage (C-G-V) measurements were done to estimate the number and polarity of fixed insulator charges (Q<sub>f</sub>). The density of interface defects (D<sub>it</sub>) was estimated from capacitance vs. conductance and frequency (C-G-f) measurements. This study evidences that the deposition of the insulators at high temperatures (300 °C) and the use of sputtering technique cause surface modification on the CIGS surface. We found that, by varying the SiO<sub>x</sub> deposition parameters, it is possible to have opposite charges inside the insulator, which would allow its use in different device architectures. The material with lower D<sub>it</sub> values was Al<sub>2</sub>O<sub>3</sub> when deposited by sputtering.

**Index Terms**— chemical passivation, Cu(In,Ga)Se<sub>2</sub> (CIGS), field-effect passivation, interface, passivation, solar cells, thin films

## I. INTRODUCTION

CURRENTLY, thin film solar cells based on Cu(In,Ga)Se<sub>2</sub> achieve an impressive world record of power conversion efficiency of 22.8 % [1]. With material quality being the improvement of choice in the last decade for CIGS technology, in recent years a bigger focus improving the interface quality has been made. At the front interface, a post deposition treatment (PDT) that is constituted by the incorporation of alkali elements reduces the front interface recombination significantly [2]–[6]. While the exact mechanisms of the PDT process that lead to an increase in the electrical performance of the solar cells and its full effects are still being discussed, a

study has shown that there is a formation of a nano-patterned layer [7]. At the rear interface, the introduction of a nano-patterned insulator layer that passivates the interface led to improvements in the power conversion efficiency of ultrathin CIGS solar cells of up to 2 % [8]–[14]. In those cases the point contacts assure electrical contact while the passivation is made by an insulator made of Al<sub>2</sub>O<sub>3</sub>. The insulator materials have the potential to passivate the CIGS interface by lowering the number of interface defects, called chemical passivation, and by creating a built-in electrical field that repels carriers, called field-effect passivation [15], [16]. For the first studies, Al<sub>2</sub>O<sub>3</sub> was the material of first choice as it is one of the best passivating materials in Si technology. For CIGS, an investigation of other oxide materials was performed as buffer layers in different solar cells configurations [17], [18] and as passivation layer [19] with different insulators than those studied in this work.

We report the study of several insulator materials, namely Al<sub>2</sub>O<sub>3</sub>, SiO<sub>x</sub> and Si<sub>3</sub>N<sub>x</sub>, to be used as passivation materials in CIGS solar cells. For this purpose, we use an inverted metal-insulator-semiconductor (MIS) structure: SLG/Mo/CIGS/insulator/Al with the rear contact made of Mo. This architecture has the advantage that the CIGS growth is done in a similar way as for regular solar cells and the disadvantage that it does not allow for annealing of the insulator layers as it might cause CIGS surface modification which can lead to interpretation problems. The annealing can change the insulator properties, namely the polarity of the fixed insulator charges Q<sub>f</sub>, and reduce the number of interface defects D<sub>it</sub> [20]. Hence, our study is relevant for cases where no annealing of the insulators is made, which is the case of alternative CIGS architectures, such as superstrate [21] or novel ones. Besides applying MIS measurements for the determination of interface traps density and fixed insulator charges concentration and electrical polarity, we also focus our attention in understanding

J.M.V. Cunha and P.M.P. Salomé acknowledge the funding of Fundação para a Ciência e a Tecnologia (FCT) through the project IF/00133/2015. B. Vermang has received funding from the European Research Council (ERC) under the European Union's Horizon 2020 research and innovation programme (grant agreement no. 715027). The European Union's Horizon 2020 research and innovation programme ARCI-GS-M project (grant agreement no. 720887) is acknowledged. J. P. Teixeira and J. P. Leitão acknowledge the funding of FCT through the project UID/CTM/50025/2013.

J. M. V. Cunha and J. Gaspar are with INL – International Iberian Nanotechnology Laboratory, Avenida Mestre José Veiga, 4715-330 Braga, Portugal (e-mail: jose.cunha@inl.int and joao.gaspar@inl.int).

P. A. Fernandes is with INL – International Iberian Nanotechnology Laboratory, Avenida Mestre José Veiga, 4715-330 Braga, Portugal, with CIETI, Departamento de Física, Instituto Superior de Engenharia do Porto, Instituto Politécnico do Porto, Rua Dr. António Bernardino de Almeida, 431, 4200-072 Porto, Portugal and with I3N, Universidade de Aveiro, 3810-193 Aveiro, Portugal (e-mail: pafernandes@ua.pt).

B. Vermang, S. Garud and D. Buldu are with University of Hasselt – partner in Solliance, Agoralaan gebouw H, Diepenbeek, 3590, Belgium, with Imec – partner in Solliance, Kapeldreef 75, Leuven, 3001, Belgium and with Imomec – partner in Solliance,

Wetenschapspark 1, Diepenbeek, 3590, Belgium. (e-mail: Bart.Vermang@imec.be; siddhartha.garud@helmholtz-berlin.de and Dilara.Gokcen.Buldu@imec.be).

A. Hultqvist and M. Edoff are with Ångström Laboratory, Solid State Electronics, Ångström Solar Center, Uppsala University, SE-751 21 Uppsala, Sweden (e-mail: adam.hultqvist@angstrom.uu.se and Marika.Edoff@angstrom.uu.se).

J. P. Teixeira and J. P. Leitão are with I3N, Universidade de Aveiro, 3810-193 Aveiro, Portugal and with Departamento de Física, Universidade de Aveiro, Campus Universitário de Santiago, 3810-193 Aveiro, Portugal (e-mail: jenniferpassos@ua.pt and joaquim.leitao@ua.pt).

S. Bose is with INL – International Iberian Nanotechnology Laboratory, Avenida Mestre José Veiga, 4715-330 Braga, Portugal and with Ångström Laboratory, Solid State Electronics, Ångström Solar Center, Uppsala University, SE-751 21 Uppsala, Sweden (e-mail: sourav.bose@inl.int).

P. M. P. Salomé is with INL – International Iberian Nanotechnology Laboratory, Avenida Mestre José Veiga, 4715-330 Braga, Portugal and with Departamento de Física, Universidade de Aveiro, Campus Universitário de Santiago, 3810-193 Aveiro, Portugal (e-mail: Pedro.Salome@inl.int).

how the deposition conditions influence or cause CIGS surface modification.

## II. EXPERIMENTAL

The main focus of this work is the study of the effects of several insulators, namely  $\text{Al}_2\text{O}_3$ ,  $\text{Si}_3\text{N}_x$  and  $\text{SiO}_x$  on the CIGS interface properties. The samples started as soda-lime glass substrate, Mo rear contact (thickness of 350 nm),  $\text{Cu}(\text{In}_{1-x}\text{Ga}_x)\text{Se}_2$  as absorber layer (thickness of 2  $\mu\text{m}$ ) and CdS (thickness of 70 nm). The CdS was deposited on top of CIGS to prevent air exposure of the CIGS during handling [22], [23]. The deposition of these layers were according to the Ångström solar cell baseline [24]. The samples names used henceforward are presented in TABLE I.

TABLE I  
SAMPLE NAMING. LF MEANS LOW-FREQUENCY DEPOSITION AND HF, HIGH-FREQUENCY DEPOSITION.

Sample Name	Sample Description	Structure
Ref	CIGS reference sample	SLG/Mo/CIGS/CdS
$\text{Al}_2\text{O}_3 - \text{S}$	$\text{Al}_2\text{O}_3$ deposited by sputtering	SLG/Mo/CIGS/ $\text{Al}_2\text{O}_3$
$\text{Si}_3\text{N}_x$	$\text{Si}_3\text{N}_x$ deposited by PECVD at 150 °C, HF	SLG/Mo/CIGS/ $\text{Si}_3\text{N}_x$
$\text{Al}_2\text{O}_3 - \text{ALD}$	$\text{Al}_2\text{O}_3$ deposited by ALD	SLG/Mo/CIGS/ $\text{Al}_2\text{O}_3$
$\text{SiO}_x - 300\text{ }^\circ\text{C}$	$\text{SiO}_x$ deposited by PECVD at 300 °C, HF	SLG/Mo/CIGS/ $\text{SiO}_x$
$\text{SiO}_x - 150\text{ }^\circ\text{C, HF}$	$\text{SiO}_x$ deposited by PECVD at 150 °C, HF	SLG/Mo/CIGS/ $\text{SiO}_x$
$\text{SiO}_x - 150\text{ }^\circ\text{C, LF}$	$\text{SiO}_x$ deposited by PECVD at 150 °C, LF	SLG/Mo/CIGS/ $\text{SiO}_x$

Before the insulator deposition, a 10 % (w/w) HCl etch was done during 2 min to remove the CdS layer and to leave the CIGS surface pristine [25]. Subsequently, the samples were taken to the deposition tools in a matter of seconds to avoid CIGS air exposure.

The insulators were deposited with 50 nm and using different techniques: i)  $\text{Al}_2\text{O}_3$  by RF sputtering at 1500 W, Ar injection with a flow of 200 sccm and deposition pressure of  $5 \times 10^{-3}$  mbar; ii)  $\text{Si}_3\text{N}_x$  by Plasma Enhanced Chemical Vapor Deposition (PECVD) at 150 °C, High Frequency (HF) of 13.56MHz, plasma power of 30 W and as precursor gases  $\text{NH}_3$ ,  $\text{SiH}_{4.5}$  and  $\text{N}_2$ ; iii)  $\text{SiO}_x$  by PECVD at three different deposition conditions: a) 300 °C, HF, plasma power of 30 W and as precursor gases  $\text{N}_2\text{O}$ ,  $\text{SiH}_{4.5}$  and  $\text{N}_2$ ; b) 150 °C, HF, plasma power of 30 W and as precursor gases  $\text{N}_2\text{O}$ ,  $\text{SiH}_{4.5}$  and  $\text{N}_2$ ; c) 150 °C, Low Frequency (LF) of 380kHz, plasma power of 60 W and as precursor gases  $\text{N}_2\text{O}$ ,  $\text{SiH}_{4.5}$  and  $\text{N}_2$ ; iv)  $\text{Al}_2\text{O}_3$  by atomic layer deposition (ALD) at 200 °C, using as precursor gases Trimethyl aluminum (TMA) as aluminum source and  $\text{H}_2\text{O}$  as oxygen source.

To create the MIS structure, metal aluminum layer contacts were deposited by thermal evaporation, with a thickness of 400 nm. The final scheme of one MIS structure and a representative SEM cross-section are depicted in Fig. 1. Each sample had 10 circular contacts with diameters of 1 mm, 5 contacts with diameters of 2 mm and 6 contacts with diameters of 3 mm.

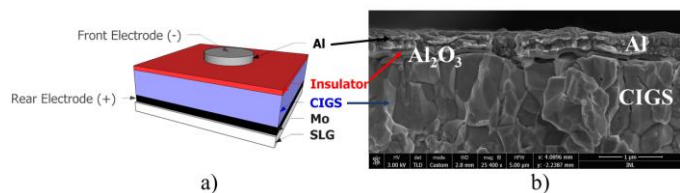


Fig. 1. a) Scheme of MIS structure: SLG/Mo/CIGS/insulator/Al. The molybdenum thickness is 350 nm, the CIGS is 2  $\mu\text{m}$ , the insulator 50 nm and the aluminum layer 400 nm (bilayer of 200 nm each). The image is not at scale. b) SEM cross-section of sputtered  $\text{Al}_2\text{O}_3$ .

Raman spectroscopy was performed, using a Confocal Raman Microscope 300 R (WiTec) with green laser (excitation wavelength of 532 nm), 1 mW of power and a Zeiss objective of 100x in the backscattering configuration. Photoluminescence (PL) was performed with a YAG, class 3B laser with a 15 kHz repetition rate and 1 ns pulse length with a beam spot of 3 mm and excitation wavelength of 532 nm. An average illumination intensity of 1 mW was used. Scanning electron microscopy (SEM) cross-section was carried out, using a NovaNanoSEM 650 tool with an acceleration voltage of 3 kV.

C-G-f measurements were done using an Agilent E4890 A with 30 mV ( $V_{\text{RMS}}$ ), 0  $V_{\text{bias}}$  from 20 Hz to 1 MHz in frequency. C-G-V measurements were done in the same tool with 30 mV ( $V_{\text{RMS}}$ ) and a frequency of 10 kHz. The ac electrical behavior of the MIS structures for the referred frequency range, was modeled using ZSimpWin 3.50 software [26], where different equivalent circuits were tested. The software fits impedance data by varying resistance and capacitance values of a user defined model circuit.

## III. RESULTS AND DISCUSSION

### A. CIGS surface modifications

One of the objectives of this study was to understand if the deposition of the insulators caused any surface modifications to the CIGS. In order to study surface morphological changes, Raman spectroscopy was performed and representative curves are shown in Fig. 2.

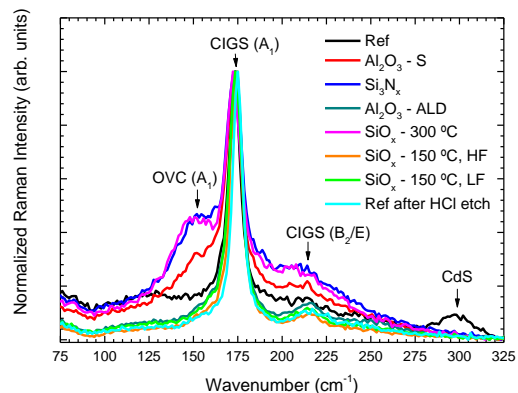


Fig. 2. Representative Raman spectra of all samples.

All the samples reveal the CIGS  $A_1$  mode peak located at 172  $\text{cm}^{-1}$  [27]. However, some of the samples, but not the reference one, show a shoulder in the low energy side of the referred CIGS peak. The shoulder, accordingly to the literature, is directly related with an order vacancy compound (OVC) [27], [28].  $\text{Al}_2\text{O}_3 - \text{S}$ ,  $\text{Si}_3\text{N}_x$  and  $\text{SiO}_x - 300\text{ }^\circ\text{C}$  samples show the

OVC layer hinting to the fact that there was some surface modification during the insulator deposition whereas  $\text{Al}_2\text{O}_3$  – ALD and both  $\text{SiO}_x$  deposited at  $150^\circ\text{C}$  do not seem to cause modification to the CIGS surface, within the precision and accuracy limits of this equipment.

A probable reason for the OVC layer appearance is a CIGS surface modification [27] which could possibly be related to: i) the high energy sputtering method; ii) the high temperatures involved in the insulator deposition ( $300^\circ\text{C}$ ); or iii) the HCl etch.

It is known that sputtering causes CIGS surface modification [29], [30] while the HCl etch should not cause any surface change [25]. To understand if the HCl etch caused CIGS surface modification, a Raman measurement was conducted before and after the HCl etching. The spectra of the reference sample and the etched sample show the same peaks, thus, it is safe to conclude that the HCl etch is not affecting the CIGS surface.

PL was used to qualitatively study the CIGS opto-electronic properties, as shown in Fig. 3. In general, more recombination channels result in a wider emission and in an increase in the number of emission peaks, which ultimately lead to a worse solar cell electrical performance [31]–[33]. Both  $\text{SiO}_x$  samples deposited at  $150^\circ\text{C}$  and the  $\text{Al}_2\text{O}_3$  sample deposited by ALD have only one narrow emission peak. The samples  $\text{Al}_2\text{O}_3$  – S,  $\text{Si}_3\text{N}_x$  and  $\text{SiO}_x$  –  $300^\circ\text{C}$  show broad emissions. Consequently, a higher number of recombination channels should be present in the latter samples compared with the former ones. Besides having a narrow emission, both  $150^\circ\text{C}$ ,  $\text{SiO}_x$  samples have a blue shift in energy of its peak position as compared with the emission from the reference sample. Such blue shift can either represent a higher bandgap value (unlikely due to the same CIGS processing in these samples) or passivation of shallow defects [34], [35]. The  $\text{Al}_2\text{O}_3$  – S,  $\text{Si}_3\text{N}_x$  and  $\text{SiO}_x$  –  $300^\circ\text{C}$  samples have an emission which is characterized by two peaks. One of the peaks is located at the same energy as the one found in the reference sample and a second peak located at higher energetic positions. It is clear that the samples with the  $\text{SiO}_x$  deposited at  $150^\circ\text{C}$  and the  $\text{Al}_2\text{O}_3$  deposited by ALD have a lower number of recombination channels affecting their electronic structure, a behavior similar to the reference sample but with different values of full width at half maximum (FWHM). To summarize the PL data, the samples that show several peaks, are likely to have several recombination channels, whereas the ones with the emission similar to the reference sample, kept the same recombination mechanism.

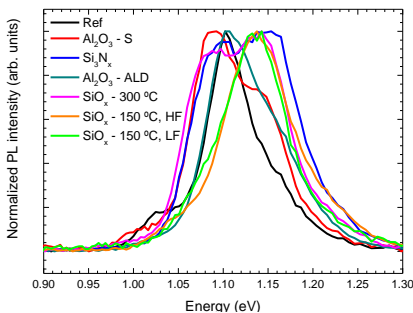


Fig. 3. Photoluminescence spectra of all samples.

A clear relation between Raman and PL measurements is observable: for  $\text{Al}_2\text{O}_3$  – S,  $\text{Si}_3\text{N}_x$  and  $\text{SiO}_x$  –  $300^\circ\text{C}$  samples,

CIGS-surface modifications are likely present. These samples involve deposition methods that are energetic and high temperature processing, hence, there is enough energy to induce surface modifications. The other samples, presenting similar PL and Raman results with the reference sample, indicate no CIGS surface modification.

### B. Interface electrical measurements

To study the insulators passivation effect, two parameters were estimated: fixed insulator charges,  $Q_f$ , and interface defects density,  $D_{it}$ , in the CIGS-insulator interface.

The fixed insulator charges,  $Q_f$ , is estimated using the following equation [36]:

$$Q_f = \frac{C_{in}(\phi_{MS} - V_{fb})}{A \times q} \quad (1)$$

where  $A$  is the front metal contact area,  $q$  is the elementary charge,  $C_{in}$  is the insulator capacitance,  $V_{fb}$  is the flat-band voltage.  $\phi_{MS}$  is the work function difference between metal and semiconductor and can be determined by [19], [36]:

$$\phi_{MS} = \phi_M - \left( \chi + \frac{E_g}{2} + \frac{kT}{q} \ln \frac{N_a}{n_i} \right) \quad (2)$$

$$n_i = \sqrt{N_c N_v e^{-\frac{E_g}{kT}}} \quad (3)$$

where  $\phi_M$  is the aluminum work function, (4.26 eV [37]),  $\chi$  is the CIGS electron affinity (4.25 eV [38]),  $E_g$  is the CIGS bandgap (1.15 eV [24]),  $k$  is the Boltzmann constant,  $T$  is the temperature,  $N_a$  is the acceptor concentration ( $5 \times 10^{15} \text{ cm}^{-3}$  [19], [20]),  $n_i$  is the intrinsic carrier concentration, being calculated using equation (3) [19],  $N_c$  is the conduction-band density of states ( $7 \times 10^{17} \text{ cm}^{-3}$ ) and  $N_v$  is the valence-band density of states ( $1.5 \times 10^{19} \text{ cm}^{-3}$ ) [19], [39]. We note that when possible these values were experimentally calculated with CIGS fabricated in the same conditions as of this study and in these conditions,  $\phi_{MS}$  reaches a value of -0.97 V. However, it is expected some variability in the Al work function, as well as, in the CIGS affinity values due to Ga content profile. We tested this hypothesis by changing  $\phi_M$  from 4.06 eV to 4.26 eV and  $\chi$  from 4.25 eV to 4.5 eV and only minor changes to  $\phi_{MS}$  were observed. Despite this evidence, as  $\phi_{MS}$  is used to calculate  $Q_f$  its absolute values should be seen with care, instead a comparison can be performed, as the CIGS and the aluminum is the same in all samples. In order to use equation (1), it is assumed that other insulator charges have a reduced effect on the  $Q_f$  measurements and that the interface traps plays a negligible role [36], a common assumption in the literature but that has yet to be fully proved [40]–[42].

C-V-f measurements were done to determine the  $C_{in}$  and  $V_{fb}$  parameters necessary to the calculation of  $Q_f$ .  $C_{in}$  is the insulator capacitance value extracted from the strong accumulation regime in the C-V curve. Taking into account the CIGS p-type conductivity, the accumulation regime is found at negative bias. To get the values of flat-band voltage ( $V_{fb}$ ), the graphical method [43] is used and the following equation is considered:

$$\left(\frac{C_{in}}{C_m}\right)^2 - 1 = 0 \quad (4)$$

where  $C_{in}$  is the insulator capacitance value, extracted in the C-V strong accumulation regime, and  $C_m$  is the measured capacitance.

A representative graph of the  $C_{in}$  and flat-band voltage ( $V_{fb}$ ) extraction is shown in Fig. 4.

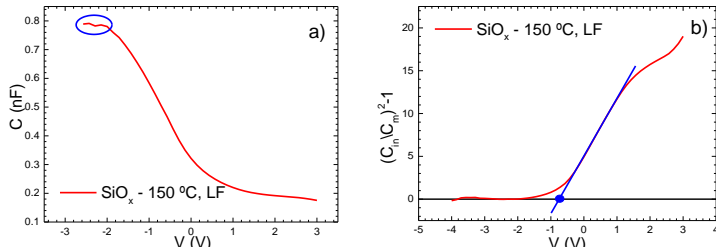


Fig. 4. Sample SiO<sub>x</sub> - 150 °C, LF. MIS with front contact of 1 mm: a) Representative C-V curve. The blue circle corresponds to the region where the  $C_{in}$  value is extracted; b) Representative  $V_{fb}$  extraction through the graphical method. The intercept of the fitted slope corresponds to  $-0.66$  V.

Averages and standard deviation for the  $Q_f$  values of the MIS structure with front contact diameter of 1 mm are found in TABLE II. The large area MIS were not measured for reasons explained further in the text.

TABLE II:  $Q_f$  VALUES TAKING INTO ACCOUNT THE AVERAGE  $C_{in}$  AND  $V_{fb}$ , MIS WITH FRONT CONTACT DIAMETER OF 1 mm.

	$Q_f \times 10^{11} (cm^{-2})$
$Al_2O_3 - S$	+3.6
$Si_3N_x$	+3.2
$Al_2O_3 - ALD$	+4.1
$SiO_x - 300\text{ }^\circ C$	+4.0
$SiO_x - 150\text{ }^\circ C, HF$	+2.8
$SiO_x - 150\text{ }^\circ C, LF$	-0.6

It is necessary to understand that the Reference sample does not form a MIS structure, hence, it was not possible to calculate the electrical parameters such as the  $Q_f$  and the  $D_{it}$ . Considering TABLE II, it was expected that the same material had the same polarity of the fixed charges, as it is shown for the  $Al_2O_3$  samples. However, an interesting observation is that for  $SiO_x - 150\text{ }^\circ C$  by changing frequency, in the deposition, it is possible to invert the polarity of the fixed insulator charges. Moreover, the insulator with positive charges ( $SiO_x - 150\text{ }^\circ C, HF$ ) can be used in solar cells architectures that prefer field-effect passivation for holes, while the insulator with negative charges are more appropriate for rear passivation of current CIGS solar cells architectures as their field-effect passivation should repel electrons.

This preliminary analysis shows that the interface  $Q_f$  values are not intrinsic to each insulator and that its concentration can be modified with growth properties.

The studied MIS structures had diameters of 1, 2 and 3 mm. However, during some of the C-V measurements, untypical behaviors appeared for the 2 and 3 mm MIS devices. Untypical behaviors of the large contact area devices observed were

caused by a resistive behavior instead of a single capacitive one. An ideal MIS structure can be characterized by the equivalent circuit represented in Fig. 5 a). In this circuit,  $C_p$  and  $G_p$  correspond to the frequency-dependent capacitance and the frequency-dependent conductance, respectively, associated to the interface-traps whereas  $C_{in}$  is the capacitance created by the insulator [36], [44], [45]. In such ideal equivalent circuit, shunt conduction in the insulator is neglected which can be a problem for leaking current in the capacitor. In that case, a more realistic equivalent circuit would be the one represented by Fig. 5 b), where a  $G_s$  is now present. However, for the case of Fig. 5 b), there are still no established models for parameters extraction with these circuit conditions. To identify if our devices were being heavily affected by insulator shunts, measured the frequency dependent impedance behavior. Afterwards, this data was fitted to the equivalent circuit of Fig. 5 b), and values of  $G_s$  were extracted using the software ZSimpWin, which provide us with values of each electric component present in the circuit. Such procedure is needed as the measurement device considers the equivalent circuit shown in Fig. 5 c) and the measured values are  $C_m$  and  $G_m$ .

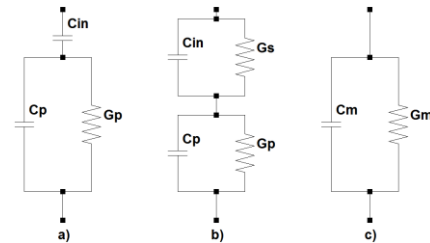


Fig. 5. Equivalent MIS circuits for conductance measurements: a) including interface-trap effect [45]; b) Same circuit of a), considering a possible series conductance; c) device's measured circuit.

The extracted values for series conductance,  $G_s$ , are shown in TABLE III. As hinted from the C-V measurements, the series conductance values increase with increasing contact diameter. These results indicate that while for small font contact diameters the electrical measurements are consistent with the circuit represented in Fig. 5 a), this is not the case for the other diameters. The results for 3 mm of the  $Al_2O_3 - ALD$  sample are not represented since the error values were too high, showing the need for even more complex equivalent circuits. Henceforth, only results for 1 mm MIS structures will be shown.

TABLE III: AVERAGE AND STANDARD DEVIATION OF SERIES CONDUCTANCE FOR DIFFERENT TOP CONTACT DIAMETERS.

$G_s (nS)$	1 mm	2 mm	3 mm
$Si_3N_x$	$20.9 \pm 6.70$	$92.9 \pm 26.2$	$(1.34 \pm 0.28) \times 10^5$
$Al_2O_3 - ALD$	$2.77 \pm 1.25$	$14.7 \pm 12.6$	-
$SiO_x - 300\text{ }^\circ C$	$11.3 \pm 1.70$	$38.0 \pm 5.00$	$146 \pm 49.0$
$SiO_x - 150\text{ }^\circ C, HF$	$25.4 \pm 17.1$	$302 \pm 201$	$1.00 \times 10^3$
$SiO_x - 150\text{ }^\circ C, LF$	$17.2 \pm 6.70$	$103 \pm 11.0$	$302 \pm 54.0$

Another important parameter for interface passivation is the density of interface defects ( $D_{it}$ ). For a comparison between the  $D_{it}$  values of each sample, the conductance method, introduced by Nicollian and Brews [44] was used. This method does not

assume the leakage current through the insulator, thus,  $G_s$  does not appear in equation (5). The value  $G_p$  for the ideal MIS structure represented on Fig. 5 a), is given by [44], [45]:

$$\left(\frac{G_p}{\omega}\right) = \frac{\omega G_m C_{in}^2}{G_m^2 + \omega^2(C_{in} - C_m)^2} \quad (5)$$

where  $\omega$  is the angular frequency,  $G_m$  and  $C_m$  are the measured conductance and capacitance, respectively, and  $C_{in}$  is the capacitance of a C-V curve measured in the strong accumulation regime [36], [44], [45]. Plotting  $(G_p/\omega)$  against frequency,  $f$ , will yield a maximum in the energy loss mechanism [20], [45] as shown in a representative plot in Fig. 6. The relation is given by [20], [36]:

$$D_{it} = \left(\frac{2.5}{A \times q}\right) \left(\frac{G_p}{\omega}\right)_{max} \quad (6)$$

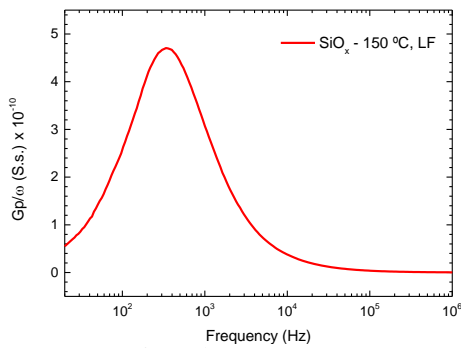


Fig. 6. Representative  $(G_p/\omega)$  against  $f$  curve of sample  $\text{SiO}_x - 150^\circ\text{C}$ , LF. MIS with 1 mm.

The extracted  $D_{it}$  values are summarized in TABLE IV. Surprisingly most of the samples show  $D_{it}$  values within the same order of magnitude, being the notable exception the sputtered  $\text{Al}_2\text{O}_3$  sample. This is a remarkable result as the sputtering of  $\text{Al}_2\text{O}_3$  was shown previously to cause some surface modifications and one would expect a higher number of electrical traps compared with samples with reduced surface modifications. While we cannot discard modifications to the composition of the  $\text{Al}_2\text{O}_3$  layer itself in the sputtering deposition, the biggest difference compared with the ALD sample is the presence of an OVC layer. In the literature there are several hypothesis that the OVC layer improves the interface, like for instance due to a similar crystal structure and better band alignment [46]–[49]. Such improvement might be an explanation for the superior results achieved with the sputtered  $\text{Al}_2\text{O}_3$  sample in comparison with the ALD  $\text{Al}_2\text{O}_3$ .

There are models to represent the  $(G_p/\omega)$  data, namely the single level defects and continuous distributions of defects [36]. Fittings were done to our data, and the most suitable model in our case is the single level defect. Moreover, it was possible to extract  $D_{it}$  values through the fittings, and the values were found to be lower than the ones calculated using equation (6), however they followed exactly the same trend of the calculated values in the present paper. Such fact is a good indication that comparisons of the  $D_{it}$  values between samples are possible to be made. However, the presented values should not be considered absolute values as a more detailed analysis has to be

performed in the future to understand what is the most accurate  $D_{it}$  extraction technique.

TABLE IV:  $D_{it}$  AVERAGE AND STANDARD DEVIATION VALUES OF MIS WITH DIAMETER OF 1 mm FOR EACH SAMPLE.

$D_{it} \times 10^{12} \text{ (eV}^{-1}\text{cm}^{-2}\text{)}$	
$\text{Al}_2\text{O}_3 - S$	$0.8 \pm 0.03$
$\text{Si}_3\text{N}_x$	$1.6 \pm 1.0$
$\text{Al}_2\text{O}_3 - \text{ALD}$	$3.8 \pm 1.4$
$\text{SiO}_x - 300^\circ\text{C}$	$3.1 \pm 1.9$
$\text{SiO}_x - 150^\circ\text{C, HF}$	$5.7 \pm 3.2$
$\text{SiO}_x - 150^\circ\text{C, LF}$	$0.9 \pm 0.09$

#### IV. CONCLUSIONS

In this work we studied the influence of depositing several insulator materials on CIGS with the objective of being used as interface passivation layers. We focused our attention in two different types of effects: i) identification of CIGS surface modifications during the deposition of the insulator; and ii) comparison of the electrical effect on the interface between CIGS and passivation layer. For surface modification we identified two trends: a) the appearance of an OVC layer; and b) unchanged samples. It was shown that the deposition of the insulator with either sputtering or high temperatures ( $300^\circ\text{C}$ ) causes the appearance of an OVC layer at the CIGS surface. Such fact was probed by Raman, and also seen in PL measurements by increased number of recombination channels.

With regard to the electrical measurements of the MIS structures, we determined that large areas lead to increased shunting between the Al contact and the Mo, which had to be dealt with by using sufficiently small values of front contact area.

For the fixed insulator charges, the values were found to be similar between each other with the same positive electrical polarity, however for the  $\text{SiO}_x$  deposited by LF, the values were found to be negative. The opposite polarity of the fixed charges mean that the same insulator can be used for different passivation roles. On the subject of density of interface defects, the insulator with lower  $D_{it}$  values compared with the others insulators, was  $\text{Al}_2\text{O}_3$  deposited by sputtering. We note that a complete study of these effects has to be a continuous effort and more information, like defect energy and defect cross section, is needed in order to fully understand the effects of interface defects on the CIGS performance.

#### REFERENCES

- [1] R. Kamada *et al.*, “New world record  $\text{Cu}(\text{In,Ga})(\text{Se,S})_2$  thin film solar cell efficiency beyond 22 %,” in *2016 IEEE 43rd Photovoltaic Specialists Conference (PVSC)*, 2016, pp. 1287–1291.
- [2] G. Sozzi, S. Di Napoli, R. Menozzi, B. Bissig, S. Buecheler, and A. N. Tiwari, “Impact of front-side point contact/passivation geometry on thin-film solar cell performance,” *Sol. Energy Mater. Sol. Cells*, vol. 165, pp. 94–102, 2017.
- [3] D. Abou-Ras *et al.*, “Innovation highway: Breakthrough milestones and key developments in chalcopyrite photovoltaics from a retrospective viewpoint,” *Thin Solid Films*, vol. 633, pp. 2–12, 2017.
- [4] A. Chirilă *et al.*, “Potassium-induced surface modification of  $\text{Cu}(\text{In,Ga})\text{Se}_2$  thin films for high-efficiency solar cells,” *Nat. Mater.*,

- vol. 12, p. 1107, Nov. 2013.
- [5] P. Jackson, R. Wuerz, D. Hariskos, E. Lotter, W. Witte, and M. Powalla, "Effects of heavy alkali elements in Cu(In,Ga)Se<sub>2</sub> solar cells with efficiencies up to 22.6 %," *Phys. status solidi – Rapid Res. Lett.*, vol. 10, no. 8, pp. 583–586, 2016.
- [6] P. M. P. Salomé, H. Rodriguez-Alvarez, and S. Sadewasser, "Incorporation of alkali metals in chalcogenide solar cells," *Sol. Energy Mater. Sol. Cells*, vol. 143, pp. 9–20, 2015.
- [7] E. Avancini *et al.*, "Effects of Rubidium Fluoride and Potassium Fluoride Postdeposition Treatments on Cu(In,Ga)Se<sub>2</sub> Thin Films and Solar Cell Performance," *Chem. Mater.*, vol. 29, no. 22, pp. 9695–9704, Nov. 2017.
- [8] B. Vermang, V. Fjällström, J. Pettersson, P. Salomé, and M. Edoff, "Development of rear surface passivated Cu(In,Ga)Se<sub>2</sub> thin film solar cells with nano-sized local rear point contacts," *Sol. Energy Mater. Sol. Cells*, vol. 117, pp. 505–511, 2013.
- [9] B. Vermang *et al.*, "Employing Si solar cell technology to increase efficiency of ultra-thin Cu(In,Ga)Se<sub>2</sub> solar cells," *Prog. Photovoltaics Res. Appl.*, vol. 22, no. 10, pp. 1023–1029, 2014.
- [10] B. Vermang, V. Fjallstrom, X. Gao, and M. Edoff, "Improved Rear Surface Passivation of Cu(In,Ga)Se<sub>2</sub> Solar Cells: A Combination of an Al<sub>2</sub>O<sub>3</sub> Rear Surface Passivation Layer and Nanosized Local Rear Point Contacts," *IEEE J. Photovoltaics*, vol. 4, no. 1, pp. 486–492, Jan. 2014.
- [11] P. M. P. Salomé *et al.*, "Passivation of Interfaces in Thin Film Solar Cells: Understanding the Effects of a Nanostructured Rear Point Contact Layer," *Adv. Mater. Interfaces*, p. 1701101.
- [12] M. Schmid, P. Manley, A. Ott, M. Song, and G. Yin, "Nanoparticles for light management in ultrathin chalcopyrite solar cells," *J. Mater. Res.*, vol. 31, pp. 3273–3289, Nov. 2016.
- [13] G. Yin *et al.*, "Well-Controlled Dielectric Nanomeshes by Colloidal Nanosphere Lithography for Optoelectronic Enhancement of Ultrathin Cu(In,Ga)Se<sub>2</sub> Solar Cells," *ACS Appl. Mater. Interfaces*, vol. 8, no. 46, pp. 31646–31652, Nov. 2016.
- [14] G. Yin, M. W. Knight, M.-C. van Lare, M. M. Solà Garcia, A. Polman, and M. Schmid, "Optoelectronic Enhancement of Ultrathin CuIn<sub>1-x</sub>Ga<sub>x</sub>Se<sub>2</sub> Solar Cells by Nanophotonic Contacts," *Adv. Opt. Mater.*, vol. 5, no. 5, p. 1600637, 2017.
- [15] B. Vermang *et al.*, "Introduction of Si PERC Rear Contacting Design to Boost Efficiency of Cu(In,Ga)Se<sub>2</sub> Solar Cells," *IEEE J. Photovoltaics*, vol. 4, no. 6, pp. 1644–1649, 2014.
- [16] M. A. Green, "The Passivated Emitter and Rear Cell (PERC): From conception to mass production," *Sol. Energy Mater. Sol. Cells*, vol. 143, pp. 190–197, 2015.
- [17] T. Koida, Y. Kamikawa-Shimizu, A. Yamada, H. Shibata, and S. Niki, "Cu(In,Ga)Se<sub>2</sub> Solar Cells With Amorphous Oxide Semiconducting Buffer Layers," *IEEE J. Photovoltaics*, vol. 5, no. 3, pp. 956–961, 2015.
- [18] M. D. Heinemann *et al.*, "Amorphous oxides as electron transport layers in Cu(In,Ga)Se<sub>2</sub> superstrate devices," *Phys. status solidi*, vol. 214, no. 5, p. 1600870, 2017.
- [19] S. Garud *et al.*, "Surface Passivation of CIGS Solar Cells Using Gallium Oxide," *Phys. status solidi*, vol. 215, no. 7, p. 1700826, Apr. 2018.
- [20] R. Kotipalli, B. Vermang, J. Joel, R. Rajkumar, M. Edoff, and D. Flandre, "Investigating the electronic properties of Al<sub>2</sub>O<sub>3</sub>/Cu(In,Ga)Se<sub>2</sub> interface," *AIP Adv.*, vol. 5, no. 10, p. 107101, Oct. 2015.
- [21] M. Terheggen, H. Heinrich, G. Kostorz, F.-J. Haug, H. Zogg, and A. N. Tiwari, "Ga<sub>2</sub>O<sub>3</sub> segregation in Cu(In, Ga)Se<sub>2</sub>/ZnO superstrate solar cells and its impact on their photovoltaic properties," *Thin Solid Films*, vol. 403–404, pp. 212–215, 2002.
- [22] R. Naciri, H. Bihri, A. Rahioui, A. Mzerd, C. Messaoudi, and M. Abd-Lefdil, "The role of CdS buffer layer in CuInS<sub>2</sub> based thin film solar cells," *Phys. Chem. News*, vol. 46, pp. 21–25, Jan. 2009.
- [23] D. Regesch *et al.*, "Degradation and passivation of CuInSe<sub>2</sub>," *Appl. Phys. Lett.*, vol. 101, no. 11, p. 112108, Sep. 2012.
- [24] J. Lindahl *et al.*, "Inline Cu(In,Ga)Se<sub>2</sub> Co-evaporation for High-Efficiency Solar Cells and Modules," *IEEE J. Photovoltaics*, vol. 3, no. 3, pp. 1100–1105, 2013.
- [25] D. Liao and A. Rockett, "Cd doping at the CuInSe<sub>2</sub>/CdS heterojunction," *J. Appl. Phys.*, vol. 93, no. 11, pp. 9380–9382, May 2003.
- [26] B. Yeum, "Electrochemical Impedance Spectroscopy: Data Analysis Software," *Echem Software*, Ann Arbor, 2001.
- [27] J. Bi *et al.*, "Pulse electro-deposition of copper on molybdenum for Cu(In,Ga)Se<sub>2</sub> and Cu<sub>2</sub>ZnSnSe<sub>4</sub> solar cell applications," *J. Power Sources*, vol. 326, pp. 211–219, 2016.
- [28] J. Wang, J. Zhu, and Y. X. He, "The influence of different locations of sputter guns on the morphological and structural properties of Cu–In–Ga precursors and Cu(In,Ga)Se<sub>2</sub> thin films," *Appl. Surf. Sci.*, vol. 288, pp. 109–114, 2014.
- [29] M. Sugiyama, H. Sakakura, S.-W. Chang, and M. Itagaki, "Investigation of Sputtering Damage around pn Interfaces of Cu(In,Ga)Se<sub>2</sub> Solar Cells by Impedance Spectroscopy," *Electrochim. Acta*, vol. 131, pp. 236–239, 2014.
- [30] X. He *et al.*, "Intermixing and Formation of Cu-Rich Secondary Phases at Sputtered CdS/CuInGaSe<sub>2</sub> Heterojunctions," *IEEE J. Photovoltaics*, vol. 6, no. 5, pp. 1308–1315, 2016.
- [31] P. M. P. Salomé, J. P. Teixeira, J. Keller, T. Törndahl, S. Sadewasser, and J. P. Leitão, "Influence of CdS and ZnSnO Buffer Layers on the Photoluminescence of Cu(In,Ga)Se<sub>2</sub> Thin Films," *IEEE J. Photovoltaics*, vol. 7, no. 2, pp. 670–675, 2017.
- [32] J. P. Teixeira *et al.*, "Radiative transitions in highly doped and compensated chalcopyrites and kesterites: The case of Cu<sub>2</sub>ZnSnS<sub>4</sub>," *Phys. Rev. B*, vol. 90, no. 23, p. 235202, Dec. 2014.
- [33] T. Gokmen, O. Gunawan, T. K. Todorov, and D. B. Mitzi, "Band tailing and efficiency limitation in kesterite solar cells," *Appl. Phys. Lett.*, vol. 103, no. 10, p. 103506, Sep. 2013.
- [34] M. V Yakushev *et al.*, "Effects of D<sup>+</sup> implantation of CIGS thin films through a CdS layer," *Thin Solid Films*, vol. 387, no. 1, pp. 201–204, 2001.
- [35] R. Bacewicz, P. Zuk, and R. Trykozko, "Photoluminescence study of ZnO/CdS/Cu(In,Ga)Se<sub>2</sub> solar cells," *Opto-electronics Rev.*, vol. 11, no. 4, pp. 277–280, Dec. 2003.
- [36] D. K. Schroder, *Semiconductor Material and Device Characterization*, 3rd ed. Hoboken, NJ, USA: John Wiley & Sons, Inc., 2005.
- [37] W. M. Haynes, *CRC Handbook of Chemistry and Physics*, 96th Edition. CRC Press, 2015.
- [38] C. Frisk *et al.*, "Optimizing Ga-profiles for highly efficient Cu(In, Ga)Se<sub>2</sub> thin film solar cells in simple and complex defect models," *J. Phys. D: Appl. Phys.*, vol. 47, no. 48, p. 485104, Dec. 2014.
- [39] A. Bercegol, B. Chacko, R. Klenk, I. Laueremann, M. C. Lux-Steiner, and M. Liero, "Point contacts at the copper-indium-gallium-selenide interface—A theoretical outlook," *J. Appl. Phys.*, vol. 119, no. 15, p. 155304, Apr. 2016.
- [40] G. Dingemans, N. M. Terlinden, M. A. Verheijen, M. C. M. van de Sanden, and W. M. M. Kessels, "Controlling the fixed charge and passivation properties of Si(100)/Al<sub>2</sub>O<sub>3</sub> interfaces using ultrathin SiO<sub>2</sub> interlayers synthesized by atomic layer deposition," *J. Appl. Phys.*, vol. 110, no. 9, p. 93715, Nov. 2011.
- [41] X. Tang *et al.*, *Room temperature atomic layer deposition of Al<sub>2</sub>O<sub>3</sub> and replication of butterfly wings for photovoltaic application*, vol. 30, 2011.
- [42] R. Kotipalli, R. Delamare, O. Poncelet, X. Tang, L. A. Francis, and D. Flandre, "Passivation effects of atomic-layer-deposited aluminum oxide," *EPJ Photovoltaics*, vol. 4, p. 45107, Sep. 2013.
- [43] K. Piskorski and H. M. Przewlocki, "The methods to determine flat-band voltage V<sub>FB</sub> in semiconductor of a MOS structure," in *The 33rd International Convention MIPRO*, 2010, pp. 37–42.
- [44] E. H. Nicollian and J. R. Brews, *MOS (metal oxide semiconductor) physics and technology*. Wiley, 1982.
- [45] S. M. Sze and K. K. Ng, *Physics of Semiconductor Devices*. Hoboken, NJ, USA: John Wiley & Sons, Inc., 2006.
- [46] T. Dullweber, G. H. Anna, U. Rau, and H. W. Schock, "A new approach to high-efficiency solar cells by band gap grading in Cu(In,Ga)Se<sub>2</sub> chalcopyrite semiconductors," *Sol. Energy Mater. Sol. Cells*, vol. 67, no. 1, pp. 145–150, 2001.
- [47] T. Minemoto *et al.*, "Theoretical analysis of the effect of conduction band offset of window/CIS layers on performance of CIS solar cells using device simulation," *Sol. Energy Mater. Sol. Cells*, vol. 67, no. 1, pp. 83–88, 2001.
- [48] A. Rockett *et al.*, "Near-surface defect distributions in Cu(In,Ga)Se<sub>2</sub>," *Thin Solid Films*, vol. 431, pp. 301–306, May 2003.
- [49] C.-H. Chung, K.-H. Hong, D.-K. Lee, J. H. Yun, and Y. Yang, "Ordered Vacancy Compound Formation by Controlling Element Redistribution in Molecular-Level Precursor Solution Processed CuInSe<sub>2</sub> Thin Films," *Chem. Mater.*, vol. 27, no. 21, pp. 7244–7247, Nov. 2015.